ICAS 2021 SHANGHAI
International Council of the Aeronautical Sciences
32nd Congress of the International Council of the Aeronautical Sciences
September 6-10, 2021
Pudong Shangri-La, Shanghai, China

RAPID THEORETICAL EVALUATION OF FORMATION FLIGHT PERFORMANCE

Rodrigo Vilumbrales-Garcia[1] & Mudassir Lone[1]

[1]Dynamics, Simulation Control Group Aerospace Integration Research Centre Cranfield University, Cranfield MK43 0A

Abstract

The concept of extended formation flying is receiving significant interest within the aerospace research community due to its potential as a solution to a range of problems faced today. In this paper, the authors focus on the flight physics aspects and discuss the development of a method to provide a means of mapping regions behind the lead aircraft in terms of drag benefits and trim control deflections. It relies on a wake prediction model based on the principles of reduced order aerodynamics, namely the unsteady vortex lattice method coupled with wake descent models. This approach called the Virtual Wing Method, aims to provide a computationally cheap means to start both a cost-benefit analysis as well as a de-risking process where the results can then be used to isolate regions where higher fidelity simulation tools can be used to extract more accurate estimates. Comparison with results from the $AVE program show the suitability of this method for capturing the trends observed in high fidelity simulations and experimental data.

Keywords: Flight formation, UVLM, aerodynamics, drag reduction

1. Introduction

It's only through the diligent study of avian flight and careful observation of bird behaviour that we have been able to get a bird's eye view of our traditional aviation practices that are often subject to our deeply rooted biases and prejudices. The concept of formation flight for increased efficiency is an example of decades long diligent research and analysis of bird flight, but it is yet to be adopted in practice. Lissaman et al.[1] proved, back in the 1970s, how three birds could increment their range by up to 25% when flying in formation compared to a solo flight. Almost twenty years ago, Weimerskirch et al[2] provided evidence for a heart-beat reduction of 15% for two pelicans voyaging in formation. Not only that, but they also proved that where some birds found it difficult to keep the positions in formation, considering all the manoeuvres required for adjustments, the heart rate reductions were still significant. On the more human front, once the world economy recovers from the global pandemic, it is highly likely that the skies will return to being the congested airways of the past, in desperate need for innovative solutions for traffic management. Moreover, the need for increased efficiency at aircraft level will retain its importance until the impact of aviation on climate is well below that of other transportation sectors. Formation flight is a promising concept of operation amongst the vast array of ideas that can help address the issues of traffic management and efficiency. It stands apart mainly because it does not seem to require the development of new airframes or technologies with very low readiness levels. However, it requires a considerable amount of de-risking and still needs definitive proof for the performance benefits it promises. The approach presented in this paper aims to provide a computationally cheap means to start both a cost-benefit analysis as well as a de-risking process. This low fidelity method, called the Virtual Wing Method (VWM), helps map a coarse grid of regions behind the lead aircraft for which estimates of drag reduction, trim control deflections and changes in rolling moment coefficients are provided. The results can then be used to isolate regions where higher fidelity simulation tools can be used to extract more accurate estimates.

The first stage of every formation flight analysis involves modelling the wake vortex evolution. Several methods have been used to simulate the wake generated by a wing/tail configuration, from high-order methods LES[3] or RANS[4] to low-fidelity panel approximations [5], or experimental research [6] [7].

The main problem of high-order fidelity methods relies on the fact that the volume sizes considered on this type of experiments are large enough to require considerable computational resources. Low-fidelity methods are not able to accurately model atmospheric or dissipation conditions such as vortex descent. This wake phenomenon has been modelled using a number of methods: the most recognized of which being the work of Green[8], Sarpkaya[9] and Holzaepfel[10]. Experimental testing has been carried out, such as Idaho Falls and Memphis Field programs, conducted in the 1990s measuring vortex characteristics from towers for different aircraft types.[11] Once the wake has been developed until the distance where it encounters the follower aircraft, the interactions of the follower and the vortex have been analysed utilising several techniques. The main experimental study involving extended flight formation is the $AVE program, carried out by the US Air Force Research Lab. Flanzer et al.[6] summarize the operational analysis of two C-17 flying at extended flight formations. The study is focused on the route aspects and consider heterogeneous formations for coronet missions. Bienawski et al[7] analysed again two C-17 studying aspects such as structural effects or aircrew damage due to wake encountering. Halaas et al. [4] presented the comparison between the expected altitude/lateral coordinate and the real one for several test points, and large were seen, which proves the difficulties for the aircrew to accurately control the position of the plane inside the wake. Several numerical studies have also been done to validate the experimental results of $AVE program. Slotnick et al.[3] compared a low fidelity VLM, medium-fidelity Panel Method, and high fidelity RANS approach in formations of two and three ships. The authors found that to simulate a high fidelity model it took around 16 hours to calculate one position while, for the medium-fidelity case, 24 hours were enough to simulate 4000 locations for the following aircraft. This highlights the difficulties of accurately modelling extended flight formation in terms of computational cost. Ning[12] developed work in terms of wake decay and descent implementation, based on[13], compressibility effects, confidence intervals, and flight formation configurations.
The present study can be positioned among the low order extended flight formation studies. Here the effects of the wake vortex generated by the leader is modelled with a UVLM code and then used to quickly obtain the drag benefit results for several thousand follower aircraft locations in terms of the imposed lateral and vertical velocity planes at a determined longitudinal distance from the leader. It also overcomes one of the principal accuracy issues that arise from low-order method: the problem of accurately predicting wakes over long distances. A wake vortex decay/descent has been integrated and validated by using available experimental data. It also provides trimmed control deflections required by the follower aircraft and its effects on the total drag savings by applying classical stability derivatives and aircraft moment equations. Final validation is done via comparisons with experimental data available in the public domain.

2. Theoretical framework

2.1 Unsteady vortex lattice method

Aerodynamic calculations based on Vortex Lattice Method (VLM) assume flow physics that is incompressible, irrotational and inviscid and are fundamentally based on potential flow theory. Careful applications can generate accurate approximations[14, 15, 16, 17] for high Reynolds number subsonic cases with no boundary layer separation or stall. The reader is referred to classical text books such as that by Katz and Plotkin[18] for detailed mathematical derivation of this modelling approach. At the core of the VLM approach lies Laplace's equation:

$$\nabla^2 \phi = 0 \tag{1}$$

where $\phi = \phi(x,y,z)$ is the velocity potential function that must satisfy:

$$\nabla \phi = v \tag{2}$$

where $v = v(x,y,z)$ represents a velocity perturbation in the field that can be associated with the potential. A solution to the previous equation can be constructed using Green's identity as follows:

$$\Phi^*(x,y,z) = \frac{-1}{4\pi}[\sigma(1/r) - \mu n \nabla(1/r)]dS + \phi_\infty \tag{3}$$

where:

$$\phi_\infty = U_\infty x + V_\infty y + W_\infty z \tag{4}$$

The Unsteady VLM (UVLM) extension effectively adds a time component to the perturbation field such that $v = v(x,y,z,t)$. The total velocity (V) of the fluid at any given point is then the sum of the free stream and perturbation velocities. VLM approximates a solution for the perturbation velocity in order to satisfy the chosen boundary conditions. The main characteristic of VLM is the use of vortex rings, which consist of four straight line segments of finite length, constant strength arranged as a three-dimensional quadrilateral as shown in Figure 1. Each ring has to satisfy the aforementioned equations and are placed over the lifting surface as a tessellation lattice. The contribution of each ring is combined to obtain the fluid properties at any given point. The wake from each surface panel is developed into a wake sheet using iterative loops at each time step and introducing a shed vortex behind the trailing edge. The UVLM code used in this study has been implemented following the procedure described in Katz and Plotkin[18]. Given a vortex line segment of strength Γ, with given position vectors, the induced velocity is computed for the schematic of vortex panels shown in Figure 1.

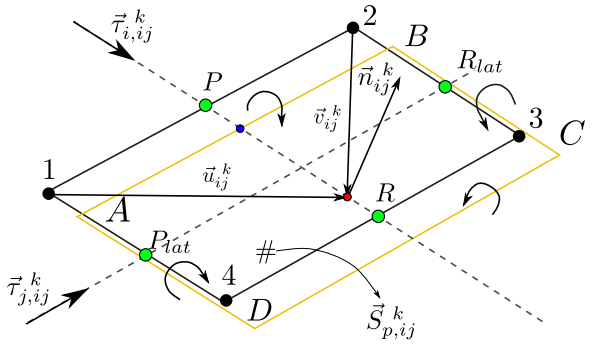

Figure 1 – Schematic of a single UVLM panel.

In order to save computational time, the aerodynamic influence coefficient (AIC) matrices that correspond to points A,B,C, and D for each lifting surface are reshaped into row vectors and added together with the others using a concatenation function. The schematic of this operation is shown in Figure 2.

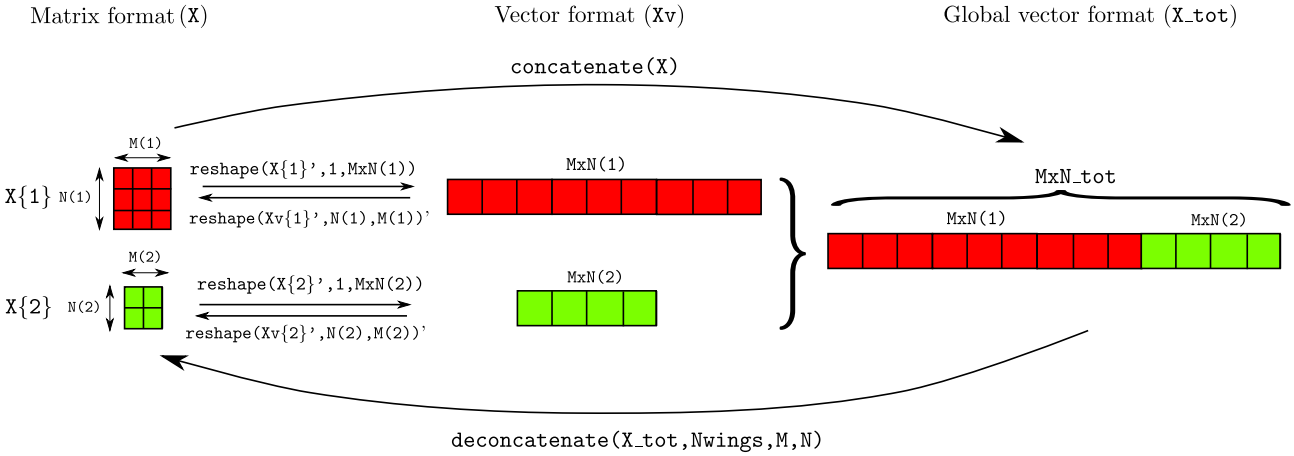

Figure 2 – Concatenation of AIRC matrices.

2.2 Wake vortex evolution

The concept of formation flight which in this study is effectively the application of Extended Flight Formation (EFF) implies large longitudinal distances between the aircraft involved, and therefore, necessitates modelling long wake development times. Considering the turbulent and sometimes chaotic characteristics of the atmosphere, it is critical to accurately model the evolution of the wake vortex in

the area between the leader and the follower aircraft. It would be an extreme simplification to assume that the wake characteristics remain constant from vortex generation to a follower aircraft's encounter with the wake. Further urgency and importance is added to this need for accurate modelling due to the fact that several accidents have happened in the past due to unexpected wake encounters. The work presented here tries to overcome the lack of accuracy of past low-fidelity formation flight approaches in terms of wake phase development by implementing a trajectory and strength correction using the well-known Sarpkaya Vortex Model[9]. This model, based on previous work be Greene[8], defines the evolution of the vortex altitude and strength as follows:

$$\frac{\Gamma}{\Gamma_0} = e^{-MT} \tag{5}$$

$$\frac{d^2Z}{dT^2} + \omega^2 N^* 2 + Me^{-MT} = 0 \tag{6}$$

where Γ is the vortex circulatiom - sub-index 0 - denotes initial value of the previous, M is Sarpkaya[9] model parameter, T, Z are the normalised time and vertical coordinate respectively, N^* is the normalised Brunt-Väisäla frequency, and ω is the angular velocity of the vortex core.
Equation 5 describes vortex circulation in terms of its initial value, time, atmospheric characteristics and generating surface details. Equation 6 defines the altitude coordinate in terms of the same parameters. Further assuming constant vortex spacing, no cross-wind, and no shear, in line with similar studies, Equation 6 can be reduced to the following exact solution:

$$Z = \frac{\omega N \sin \omega N * T - Me^{-MT} + M}{M^2 + \omega^2 N^* 2} \tag{7}$$

From Equation 7, it can be seen that the wake vortex evolution is influenced mainly by Brunt-Väisäla frequency (B-V) (N^*). Brunt-Väisäla gives the frequency of oscillation for a fluid particle displaced from equilibrium in a statically stable atmosphere. The values encountered in the atmosphere for different conditions have been widely studied, and the usually a value between 0.01 and $0.04s^1$ is used along with a mean value for winter of $0.02s^1$. Another important parameter is the eddy dissipation rate, ε^*, as it influences Sarpkaya parameter [9] and has been defined by Crow[19] for three different atmospheric turbulence conditions, $\varepsilon^* > 0.25$ (high-turbulence), $0.25 < \varepsilon^* < 0.01$ (medium-turbulence) and $0.01 < \varepsilon^* < 0.001$ (low-turbulence). It has been proven that the vast majority of flight operations fall into the latter range and so for the work presented here, ε^* has been chosen as 0.01. Once ε^* has been defined, T^* can then be introduced. This parameter, the time at which a catastrophic event occurs[19], is used to describe the theoretical life of a wake vortex in terms of the duration for which it will persist in the atmosphere before dissipation. From an operational point of view, it is unlikely that formation flight operations would occur in high-turbulence conditions, mainly due to safety reasons. Therefore, it can be assumed that the follower aircraft is going to reach the wake before T^* in all cases. Hence, the simulation and modelling of the dissipation phase is not required and has not been considered in the present work. Finally, the geometry of the wake generating wing is introduced by ω in Equation 7 using the Lamb-Ossen vortex core approximation following a similar process detailed by Katz[18], Drela[20], and Sarpkaya [9].
The present work compares the UVLM results with Memphis Study Database to validate the position of the vortex in terms of its altitude coordinate, available in Reference [21], and shown in Figure 3. The Memphis Study was a series of experimental studies that used LIDAR information to sense the wake evolution behind different types of aircraft. A flat plate approximation of a Boeing 727 wing was used to perform the validation of the approach. Figure 3 presents the time evolution of the vortex vertical position, where agreement can be seen between UVLM results, Sarpkaya theoretical approach, and Memphis experimental test data. In the present work, symmetry was assumed with respect to the longitudinal axis of the wing, so only the port vortex results are presented for the UVLM case. Also, the fact that the main parameter that influences the vortex descent is the wingspan implies no significant errors are introduced due to the flat-plate approximation. The previous figure is presented in terms of time vs altitude in line with previous studies[9].

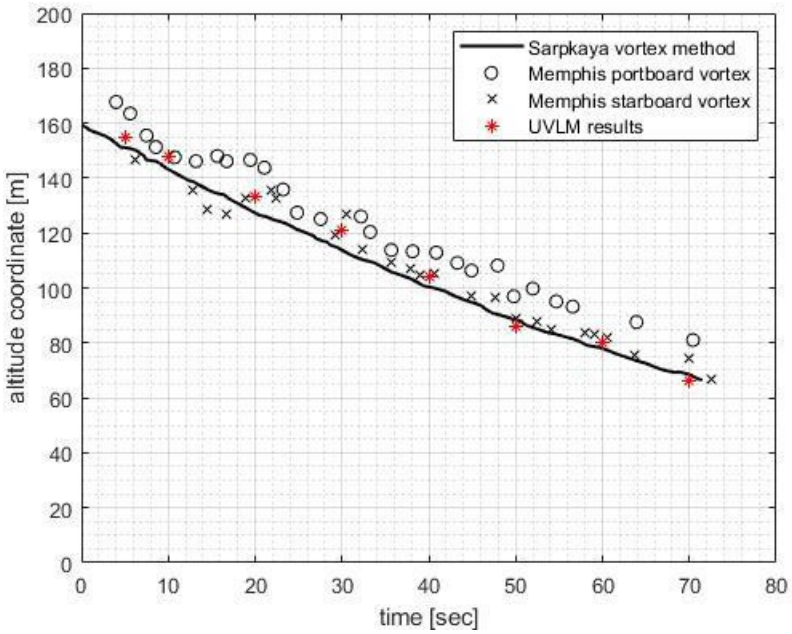

Figure 3 – Validation of wake descent model.

It is worth mentioning that the use of such a low-fidelity approach makes the method presented in this work unsuitable for high-turbulent atmospheric conditions and unsteadiness but, the implementation of a vortex evolution and descent model together with the acceptable accuracy of the results implies that the approach retains some validity in the specific cases studied in this paper. Moreover, high-fidelity approaches are not assumption-free either and incur high computational cost. It is not the aim of this study to develop a high-accuracy wake evolution method but to estimate the most-likely location of the wake vortex core to perform efficient formation flight operation.

3. Simulation setup

The modelling and simulation framework used to exercise the theoretical modelling methods and thus, support comparisons with formation flight data available in the public domain requires the integration of three aspects:

1. Wake generation and evolution: where the UVLM method is used to calculate the wake field and its evolution behind the lead aircraft.
2. Wake encounter: where the wake flow field is applied to the follower aircraft.
3. Follower aircraft trimming : where control inputs required by the follower aircraft for trimmed steady level flight conditions are calculated.

The procedures along with corresponding assumptions and approximations for each of the above aspects are further detailed individually below.

3.1 Wake generation and evolution

Wake evolution from roll-up to its encounter with the follower aircraft has been modelled using the UVLM approach described in Section 2.1. The subject aircraft, a C-17 military transport, was chosen solely to allow some degree of comparison with the flight test data published as part of the USAF $AVE program. A number of simplifications were made when implementing aircraft geometry due to the theoretical nature of this study, the limitations of the simulation framework and to a certain degree, the lack of aircraft geometry data. These simplifications are as follows:

1. Only the wings and horizontal tailplane have been implemented for the lead aircraft, and these are modelled as flat plates as shown in Figure 4.
2. The fuselage and the vertical tailplane have not been implemented.

The flat plate approximation used for the wings and horizontal tailplane was considered to be a valid simplification as long as both the lead and follower aircraft were modelled in the same way. This allows the study to focus on the relativistic comparisons where any trends observed in the results can be scrutinised and linked to the primary aerodynamic effectors. It is expected that these simplifications will introduce discrepancies in absolute values when simulation results are compared with experimental data or studies that use higher order methods. However, as shown later in Section 4, the primary trends in aerodynamic performance and wake characteristics are still captured. A further assumption that needs to be explicitly stated is that this study assumes that the fuselage has negligible impact on the wake field and its evolution, and therefore, it's omission from the simulation can be justified. However, the authors note that in reality the wake field a few fuselage lengths aft of the aircraft will be effected by the fuselage and it could pull the wing vortices more inboard and the tailplane vortices down: affecting the interaction between the wakes of the two lifting surfaces.

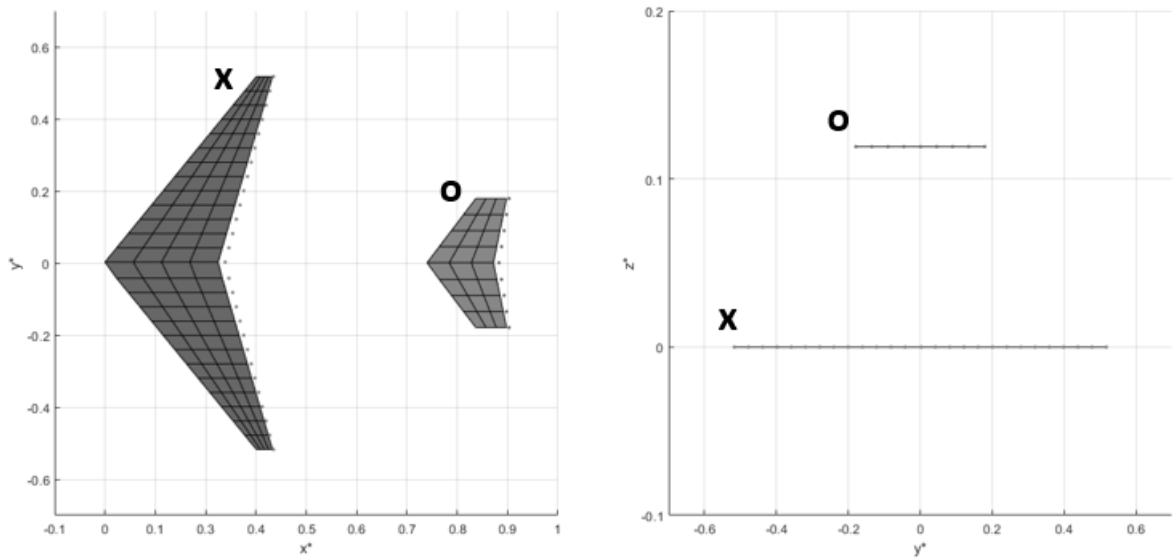

Figure 4 – Modelling of lead aircraft aerodynamics. $x^*, y^* and z^*$ are the x,y,z axis normalised with the mainwing span. The x denotes the mainwing and the o the horizontal tail surface

The evolution of the wake vortices up to a distance of approximately 30 spans (around 1500 m aft of the aircraft) can be seen in Figure 5. Here it is evident that the UVLM approach provides a quick and cheap means of studying the first order interactions between the wing and tailplane wake vortices as they evolve and travel downstream (towards a potential follower aircraft). The wing-tailplane wake interactions can be seen when the wake reaches $x^* = 20$. It is at this point where the tailplane wake starts to interact with the main wing circulation. This will be explained in detail in the Section 3.2.
It is worth mentioning at this point that the wake development phase corresponds to the most computational expensive stage of the approach detailed here. The UVLM algorithm requires the use of small time steps to avoid the growth of numerical errors in the simulations. This together with the distances required to study formation flight (up to 1500 m or 30 span lengths) increased the number of iterations needed to get a wake solution. On a typical desktop computer, up to two minutes of calculation time as required to model around 7 seconds of wake development.

3.2 Wake encounter

Earlier the authors mentioned that the computational time required for the UVLM approach to develop a wake field suited for this study was high in the context of low fidelity reduced order models. Moreover, this computational cost becomes considerably larger given that the work presented in this paper aims to obtain performance results not for one, but several follower positions. Thus, enabling the derivation of a 'drag benefit map' to identify the location of a sweet spot for the follower aircraft. This computational cost was avoided by making a further assumption: that the follower aircraft does not have any upstream effect on the wake of the lead aircraft. This effectively allows the wake field to

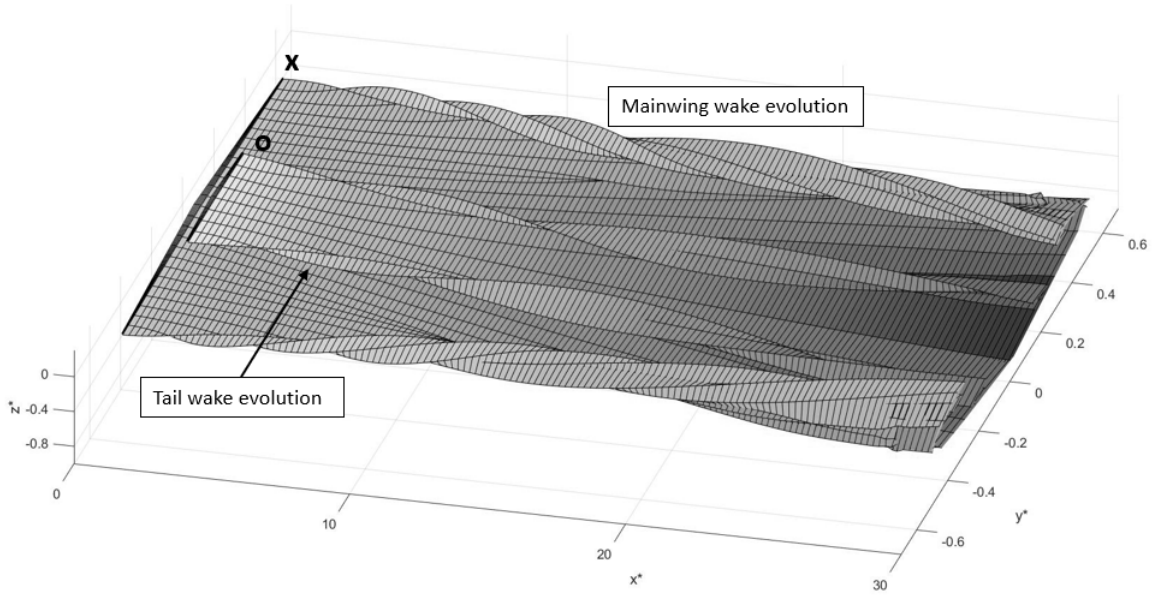

Figure 5 – Wake development phase from wake generation to encounter with follower.

be frozen at the position of the follower aircraft so that the wake effects can be simply superimposed on the wind velocity vector effecting the follower. Therefore, a single simulation computing the wake evolution can be used to evaluate the aerodynamic performance of a follower aircraft in a number of vertical and lateral positions.

The aerodynamic mechanism responsible for performance gains in formation flight has been well documented in a number of studies [5, 12, 3, 7]. Essentially, when the follower aircraft encounters the wake, the vertical velocity component added by the vortex circulation increases the effective angle of attack, rotating the aerodynamic forces vector forward, and hence reducing induced drag. This reduction in drag is due to the corrections that the follower aircraft can make after the wake encounter, mainly affecting the angle of attack attitude. As the effective angle of attack is higher, the FA can maintain the same lift at a lower α. Figure 6 schematically presents the comparison between the aircraft forces before and after the wake encounter. The modelling simplifications and assumptions made in this study are significant when one considers the variety of aerodynamic interactions occurring between the wake field and the follower aircraft. Given the subsonic flight conditions of the formation flight considered here, the upstream effects of the follower aircraft on the wake field is being ignored; especially since the fuselage is being ignored. Inclusion of the fuselage upstream effects would most likely push the wake vortex cores further outboard impacting the follower aircraft's wing lift distribution. Inaccuracies as a result of ignoring such effects are deemed acceptable by the authors because the approach detailed in this paper is seen as a preliminary means of quickly assessing a large number of follower positions to identify a sweet spot that can be validated later via higher fidelity simulations. Furthermore, the present work has not considered any other drag component apart from induced drag, similar to work presented in Reference [3]. This will result in some discrepancies with experimental or high-fidelity analysis and lead to overestimating operational benefits. Hence, the final performance results will address exclusively the effects with respect to the solo flight condition. As a second part of the present work, the effects of trimming the follower aircraft will be added, as explained later in Section 3.3. The difference in induced drag imposed by the wake is thus obtained simply as follows:

$$\Delta D = L \sin \Delta\alpha = (L + \Delta L) \sin(\Delta\alpha) \tag{8}$$

where D, L are the Drag and Lift forces respectively, and α is the effective angle of attack.

Taking advantage of this relatively simple approach, a new method called 'Virtual Wing Method (VWM)' has been developed by the authors. The first stage of VWM consists of capturing the imposed vertical and lateral velocity profiles at the required longitudinal distance with respect to the

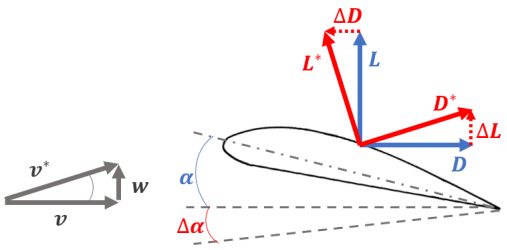

Figure 6 – Aerodynamic vector rotation. Re-drawn from [5]

leader. This allows the generation of a 2D plane in z*/y* that stores the effects of the wake at the required distance. Assuming similar conditions for all relative positions of the follower aircraft, and considering that $\Delta\alpha$ can be obtained, following Fig. 6, from those imposed vertical and horizontal velocities, the aforementioned 2D velocity plane is sufficient to obtain the instantaneous induced drag variation for as many follower locations as required. This procedure means that the wake evolution calculations that develop the wake from roll-up to encounter only needs to be carried out once, overcoming the issue of computational cost. A further assumption made at this point is that the 2D velocity plane is the same for the main wing and the tail. This implies that the effect of the main wing downwash over the horizontal tail has been ignored, but again, only high-fidelity methods are able to deal with the mentioned aerodynamic interactions, as can be seen in the discussion of the results presented by [3].
The VWM approach is presented schematically in Figure 7. On the left, the vertical velocity component of the wake at the encounter position is presented and this 2D plane is divided into a grid, where each black dot corresponds to a vertical or lateral induced velocity value. The locations of the main wing and tail vortex cores can be seen in the wake profile. The right part of the figure presents the VWM approach itself. With the information obtained from the first stage, the virtual location of the follower aircraft is defined with respect to these grid points, corresponding to a j,i coordinate indices. The virtual geometry of the follower (shown on the top right hand side of Figure 7) is divided into three vectors in terms of its spanwise projection, one for each surface, (main wing, vertical tailplane, horizontal tailplane). This allows mapping of the wake velocity vectors to a point on the follower aircraft and therefore, the calculation of the effects of the wake at each of the lifting surfaces. Then the following simple integration and area corrections can be used to sum up the overall effects:

$$\Delta L_w = \sum q_\infty a_w \Delta\alpha_i s_i - L_{w0} \quad (9)$$

$$\Delta L_t = \sum q_\infty a_w \Delta\alpha_i s_i - L_{t0} \quad (10)$$

$$\Delta Y = \sum q_\infty a_w \Delta\beta_i s_i - Y_0 \quad (11)$$

where L_w and L_t are the lift components of the mainwing and tail, q_∞ is the freestream dynamic viscosity, Y is the sideforce, β is the sideslip angle and s_i is the area of the panel.
In summary, the stages of VWM are as follows:

1. Capture the induced velocity planes at the required x^*.
2. Position the follower aircraft in terms of j,i.
3. Divide the surfaces in parts using the vectors n,b,t
4. Calculate the effects of the wake at each of the divisions, correct for the area and add them to obtain the total spanwise force distributions.
5. Change the location of the follower aircraft ($j+\Delta j, i+\Delta i$).

VWM enables the assessment of a follower aircraft performance in thousands of locations behind the lead aircraft at very low computational cost. This highlights the advantages of the VWM approach with respect to previous EFF analysis in terms of simulation cost.

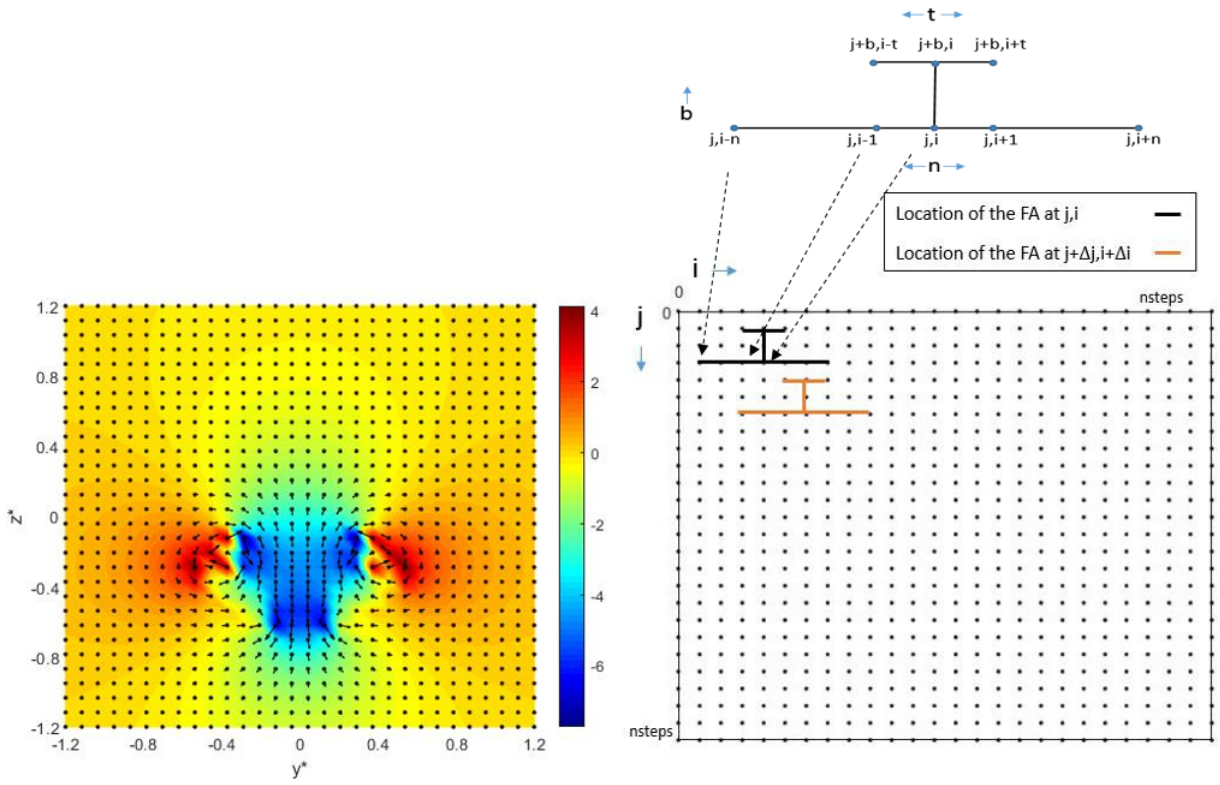

Figure 7 – Overview of Virtual Wing Method.

3.3 Aircraft trimming

After encountering the wake, the steady-state attitude of the follower aircraft is inevitably disturbed. The unsteady flow condition imposed by the vortex is expected to generate asymmetric loads over the aircraft affecting its trimmed flight condition. The procedure described here models the aircraft condition after the encounter in terms of its new incidence angle, rolling, pitching and yawing moment. The second part of this section details the analysis concerning the corrections needed for the aircraft to return to a stable condition.

The induced velocity planes presented in Figure 7, allows the approximation of the changes in the aircraft attitude using the classical stability equations [22] or the experimental tables presented in [23]. Starting with the lift coefficient, the follower aircraft perturbed coefficient is determined considering the contributions of both tail and main wing.

$$\Delta C_L = \Delta C_{L_w} + \frac{S_t}{S_w}\Delta C_{L_t} \tag{12}$$

where C_{L_w} and C_{L_t} are wing and tail lift coefficients respectively and both have been computed using Equation 9 and Equation 10. S_w and S_t are the mainwing and tail surface areas, and c is the mean mainwing chord. Next, the pitching moment C_M is obtained as follows:

$$\Delta C_M = C_{M_0} + \Delta C_{L_w}(h - h_0) - \frac{S_t l_t}{S_w c}\Delta C_{L_t} \tag{13}$$

$$C_{L_t} = a_t \alpha_t + a_t \delta_E \tag{14}$$

$$\delta_E = \alpha - \varepsilon - \eta_t \tag{15}$$

where h is the distance between the wing aerodynamic centre (h_0) and the center of gravity, δ_E is the angle of attack of the horizontal stabiliser, ε is the downwash angle, η_t is the difference in effective incidence angle between the stabiliser and wing (defined as 0 due to the assumptions of this study) and a_w, a_t are the mainwing and tail lift/alpha slope.

Assuming flat plate conditions, and assuming the follower aircraft is trimmed in a steady level flight condition prior to encountering the wake, Equation 13 can be reduced to:

$$\Delta C_M = C_{M_0} + (a_w(h-h_0) - (a_t(1-\frac{d\varepsilon}{d\alpha}))\frac{S_t l_t}{S_w c})\Delta\alpha \tag{16}$$

Next, the rolling moment (C_l) has been defined as a balance between the contribution of the main lifting surfaces - port and starboard -:

$$C_l = C_{lrw} + C_{lrt} + C_{llw} + C_{llt} + C_{l_{\delta_R}} + C_{l\Gamma} \tag{17}$$

where C_{lrw}, C_{llw} are the mainwing port and starboard lift components, C_{lrt}, C_{llt} are the tail port and starboard lift components, $C_{l_{\delta_R}}$ is the rudder component, and C_{l_Γ} is the rolling moment component that corresponds to the dihedral angle of the main wing given by:

$$C_{l\Gamma} = a_w b_{mac} \Gamma\beta \tag{18}$$

where Γ is the dihedral angle. With the flat-plate approximation, the component detailed in Equation 18 can be neglected, as it is assumed that there is no dihedral angle. While the contribution of this component to the total rolling moment is minimum, if the actual dihedral angle of the aircraft to be studied is known, it can be added to the overall process by eliminating the simplification of the term presented in Equation 18. Finally, the yawing moment variation is obtained as follows:

$$C_n = -\frac{S_r l_r}{S_w b} a_{vt}\beta \tag{19}$$

where a_{vt} is the rudder lift/alpha slope and S_r, l_r are the rudder area and length.
This assumes that the vast majority of the disturbance in this parameter comes from the effects of the wake on the vertical tail, and specifically, the vortex horizontal velocity component, the plane used for yawing (Figure 5), is the $X-Z$ plane.
Now, the wake vortex effects on the follower aircraft, and the corrections needed to return it to a stable flight can be determined. Steady-state has been defined as a flight condition where four requirements are satisfied:

$$C_L = \frac{mg}{1/2\rho V^2 S} \tag{20}$$

$$C_m = C_l = C_n = 0 \tag{21}$$

Note that it is assumed that drag is always compensated by thrust.
Now, considering the results obtained via Equations 12-19 as initial conditions, and relating the steady-state attitude to both the constraints and the control parameters, a trimming matrix equation based on the work done by Slotnick et al[3] is defined as follows:

$$\mathbf{B} = \begin{bmatrix} \Delta C_L \\ \Delta C_m \\ \Delta C_l \\ \Delta C_n \end{bmatrix} \tag{22}$$

$$\mathbf{A} = \begin{bmatrix} C_{L_\alpha} & C_{L_{\delta_E}} & C_{L_{\delta_A}} & C_{L_{\delta_R}} \\ C_{m_\alpha} & C_{m_{\delta_E}} & C_{m_{\delta_A}} & C_{m_{\delta_R}} \\ C_{l_\alpha} & C_{l_{\delta_E}} & C_{l_{\delta_A}} & C_{l_{\delta_R}} \\ C_{n_\alpha} & C_{n_{\delta_E}} & C_{n_{\delta_A}} & C_{n_{\delta_R}} \end{bmatrix} \tag{23}$$

$$\mathbf{X} = \begin{bmatrix} \Delta\alpha \\ \delta_E \\ \delta_A \\ \delta_R \end{bmatrix} \tag{24}$$

such that:

$$\mathbf{B} = \mathbf{AX} \tag{25}$$

which when rearranged for an iterative solution search:

$$\mathbf{X}^{n}_{trim} = \mathbf{A}^{-1}[\mathbf{B}_{trim} - \mathbf{B}^{n-1}_{trim}] + \mathbf{X}^{n-1}_{trim} \tag{26}$$

where δ_E,δ_A, δ_R are the elevator, aileron and rudder deflections.
This is an iterative approach that relies on varying the terms introduced in Equation 24. This process effectively determines whether the steady-state conditions are reached or not. When the steady state criteria is satisfied, it returns the effective angle of attack of the follower aircraft after the encounter and trimming phase together with the required trim control inputs. These are then used to evaluate aerodynamic performance that includes contributions due to control surface trim deflections.
The main advantage of VWM with respect to Reference [3] relies on the approach followed to define the stability derivatives matrix presented in Equation 19. Whilst the method presented in Reference [3] requires the use of six LES simulations, VWM has defined it following a theoretical approach based on the work done by Cook[22] and Hoerner[23]. The matrix $\mathbf{A}$ can be populated with a limited set of aircraft performance parameters, such as lift-slope curve or geometrical definitions. Only a preliminary study is required together with basic aircraft information. Although in the interest of retaining simplicity and minimising computational cost, only the effects of α are considered, the authors understand that the omission of the sideslip angle, β, will lead to the overestimation of performance benefits in the final results.
As seen in Equation 26, the control surfaces deflection needed to counteract the vortex effects can be estimated and then used to obtain the trim drag penalty. The present study is considering only the effects of flight formation in the induced drag of the aircraft, and other components such as the parasite drag have not been modelled.
The relationship between control surface deflections and induced drag can be implemented with the output of the iterative process. As the ailerons are deflected asymmetrically, it is assumed that their effect on induced drag penalty is negligible. Therefore, the total induced drag $C_{D,i}$ of the follower aircraft after adding the trimming effects is presented in Equation 27

$$C_{D,i} = \Delta C_{D,i} + C_{D,i_E} + C_{D,i_R} \tag{27}$$

where $\Delta C_{D,i}$ is the increment of induced drag caused by the new α, and C_{D,i_E}, C_{D,i_R} are the induced drag caused by the elevator and rudder deflection.
The results in relation to drag benefits are going to be presented in terms of a ratio between the drag produced by the leader aircraft and the follower. Values over 1 will explain that the aircraft is extracting a performance augmentation from the wake.

$$\Delta C_{D,i} = \frac{C_{D,i,follower} - C_{D,i,leader}}{C_{D,i,leader}} \tag{28}$$

4. Results

The present study focuses on the conditions reported in the $AVE flight trials which involved the formation flight of two USAF C-17s flying over the Pacific. This is because the published results are the only results available to the authors at the time when this work was being carried out. The first set of results to be presented and discussed are those that relate to the UVLM generated wake and its evolution downstream of the lead aircraft. The focus of this section then switches to the follower aircraft where the results from the wake encounter phase are discussed together with the required trim control deflections. Finally, the estimated performance benefit map derived using VWM is presented. The flight condition chosen for analysis was 225 m/s at 9000m altitude where the longitudinal separation between the aircraft is approximately 1500m.

4.1 Wake evolution phase

Figure 8 introduces the wake imposed upwash velocity at three distances from the leading aircraft: x^*=6.3, x^*=12.4, and x^*=34.5, similar to those chosen by Misaka et al[24]. The wake descent evolution with time is also evident in Figure 8. For x^*=6.3 it is roughly at the same level as the lead aircraft's lifting surfaces, but as x^* increases, it starts to descend, following a trajectory prescribed by Sarpkaya et al[9]. At x^*=12.4, around 2.9 seconds after the wake generation, the vortex of the main wing is roughly 10% (or $y* = 0.1$) of the mean aerodynamic chord below its original position. The descent effect is magnified for the tailplane wake, due to the dragging interactions with the considerably stronger main wing vortex. Finally, at x^*=34.5, around 8s after the wake generation, the main wing vortex structure is almost half a chord below its starting point.

The lateral translation (y^*) of the wake vortex structures during wake evolution do not seem to be affected much. However it is clear that main wing vortex containing greater vorticity pulls the tailplane wake outboard, in the same way as shown by Misaka et al[24]. It is worth mentioning that the results presented in Figure 8 are highly simplified. In a real scenario, the interactions between the tail and wing vortex would be considerably more complex. Although the panel model seems to capture part of this phenomena - visible at the small vorticity regions of Figure 8, similar to those presented by Fleischmann et al[25], its simplistic assumptions do not allow modelling such inter-component components in detail. The lack of a fuselage model is another source of error when comparing this simplistic approach to other studies.

4.2 Wake encounter and trimming phase

The results obtained in this study using VWM have been compared to the approach of Slotnick et al[3] OVERFLOW approach, that relies on RANS simulations. [3] data has been obtained by digitalisation of the figures presented at their paper. Considering that the VWM approach is deliberately a low fidelity method, its accuracy is far from that of Slotnick et al[3], the lack of accuracy in the direct comparison of some parameters is unavoidable. On the one hand, these discrepancies can be caused by multiple aspects, ranging from the simplicity of the UVLM model, flat plate approximations or lack of modelling of components like the fuselage. On the other hand, given the method presented in this study does not aim to provide a final estimation of wake surfing encounters and only serve as a first rapid prediction tool, the authors consider that other aspects such as the predicted trends or the locations of the peak benefits are of more interest here.

Figure 9 introduces the lift, pitch and rolling moments that the follower aircraft is subjected to during the encounter phase at a longitudinal distance $x* = 1500m$ from the leader. These aerodynamic forces and moments characteristics are introduced in terms of y^*. Starting with lift, it can be seen that, although the absolute values differ from the reference RANS based study[3]), the trend followed by the curve is similar for both models. VWM has been able to capture the peak of the imposed C_L (at $y^* = 0.8$) that corresponds roughly to the location of the main vortex, as shown earlier in Figure 8. The transition area between regions of lift generation and lift loss can be seen to be located near $y^* = 0.75$ by both approaches. This last parameter is of especial importance for safety reasons, and proves the enormous effect that an unexpected encounter can have on the follower aircraft.

Now considering the pitching moment characteristics shown in the top-right corner of Figure 9, discrepancies between RANS and VWM have been found in both absolute and relative results. The difficulties of properly capturing this effect were also discovered by Slotnick et al[3] with their medium-fidelity DACVINE method. The authors found that the lack of the modeling the complex interactions between wing downwash and the tailplane was significantly affecting the pitching moment analysis. The VWM approach is also considerably simpler than the DACVINE method, yet it can be seen that it provides a reasonable neutral point - area where the wake imposes no effects in the follower aircraft - estimation at $y^* = 0.5$, whilst overestimating the effects of the wake in the inner regions of y^*. However from the perspective of aircraft performance, these inaccuracies in pitching moment trends are not as significant as the accurate prediction of trends in lift force.

The wake-imposed rolling moment is shown at the bottom of Figure 9. It is also evident that VWM estimates similar values and trends to those obtained through RANS, particularly in the peak effects ($y^* = 0.4$) and neutral points location ($y^* = 0$ and $y^* = 0.8$). It is known that the rolling moment is

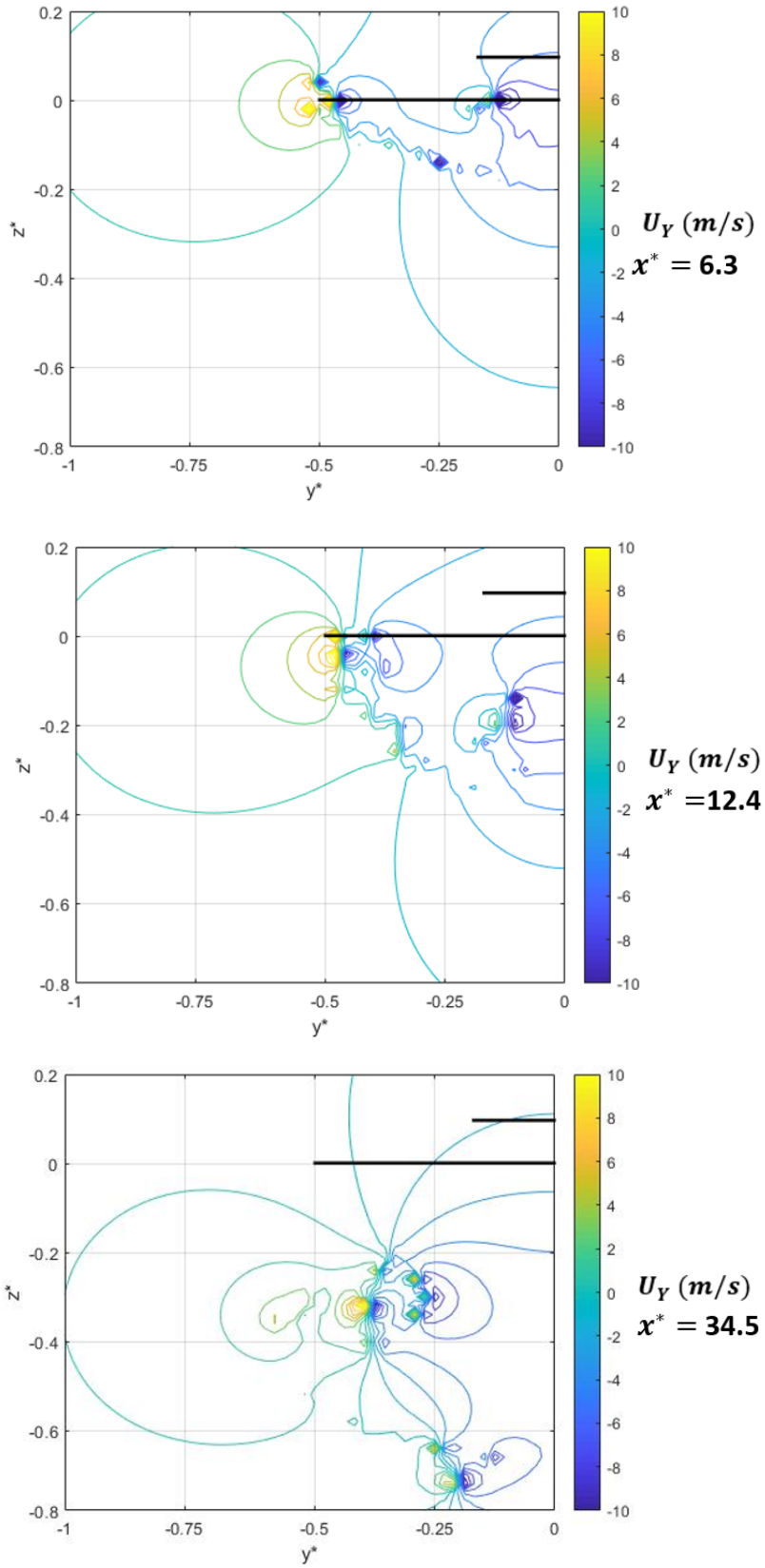

Figure 8 – Wake evolution phase at three different trailing positions. The black lines denote the position of the lead aircraft (horizontal tail and wing.)

caused mainly by a difference in lift between the port and starboard lifting surfaces. This relative difference between one side of the aircraft and the other eliminates the inaccuracies found on the lift calculation, reducing the absolute variances in rolling moment. Still, aspects such as dihedral angle

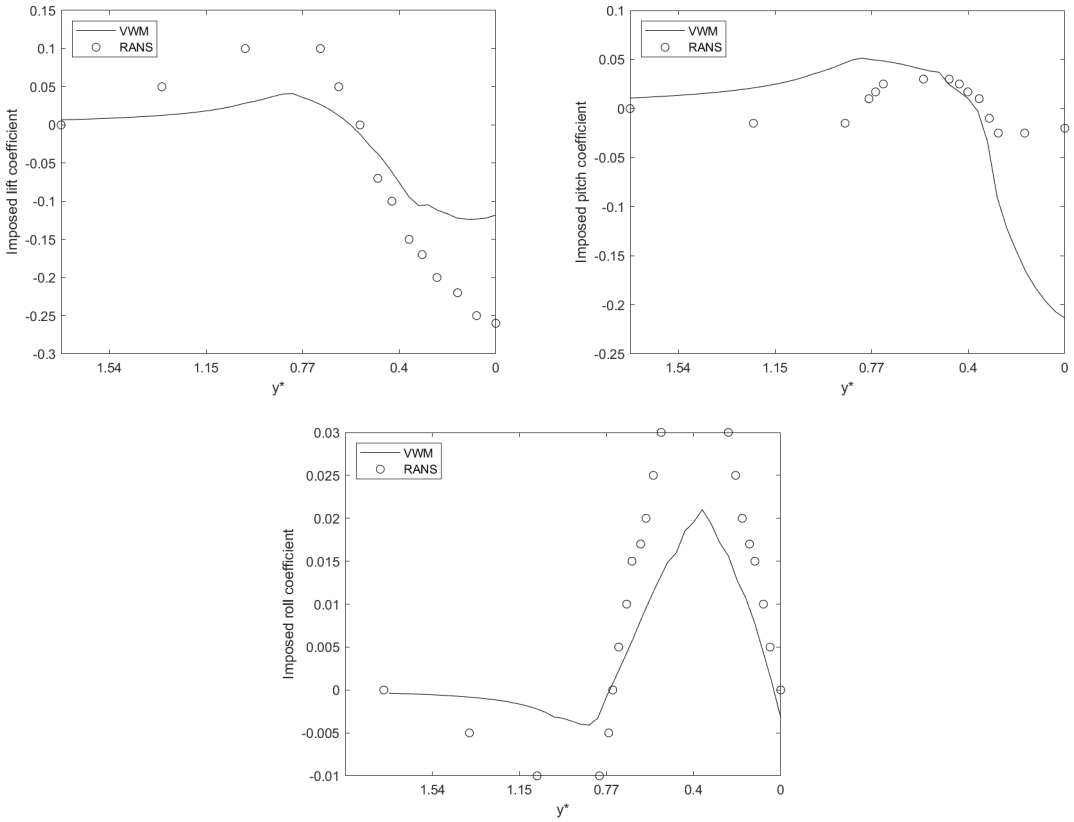

Figure 9 – Wake effects on follower aircraft forces and moments.

simplification or the effects or the tail do cause some discrepancies.

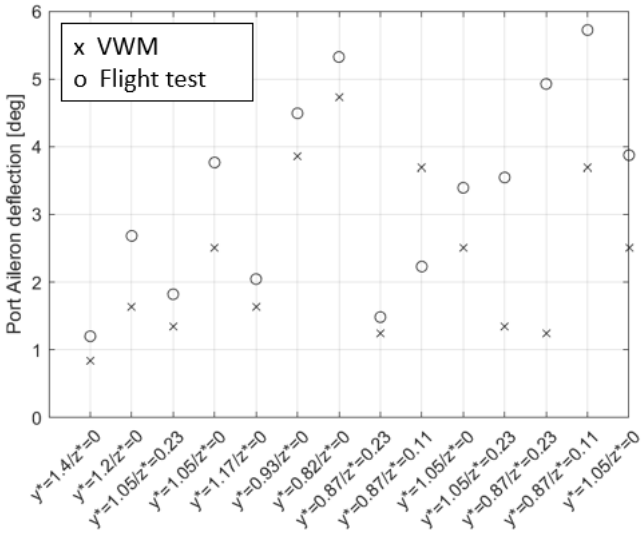

Figure 10 – Required trim aileron deflection for the follower aircraft.

.
The aileron deflection needed to counteract the effects of the wake are shown in Figure 10. The results obtained via VWM at several y^*/z^* locations are compared to the data presented by Bieniawski et al[7]. Both models show some agreement in the trends at all the points where $z^* = 0$ while, for the remaining cases, the agreement diminishes. This effect can be associated to differences in vortex core location prediction, which is not a surprise considering that the VWM model follows simple theoretical approaches which is here, being compared to data collected from experimental testing.

4.3 Performance assessment

This section covers the results concerning the drag benefits obtained during a steady state formation flight operation with no atmospheric disturbances. The drag-benefit map for such a scenario is shown in Figure 11 which corresponds to a slice at a longitudinal distance of $1500m$ or 30 wingspans from the lead aircraft. This is presented in terms of its y^*/z^* components and assumes a longitudinal plane of symmetry.

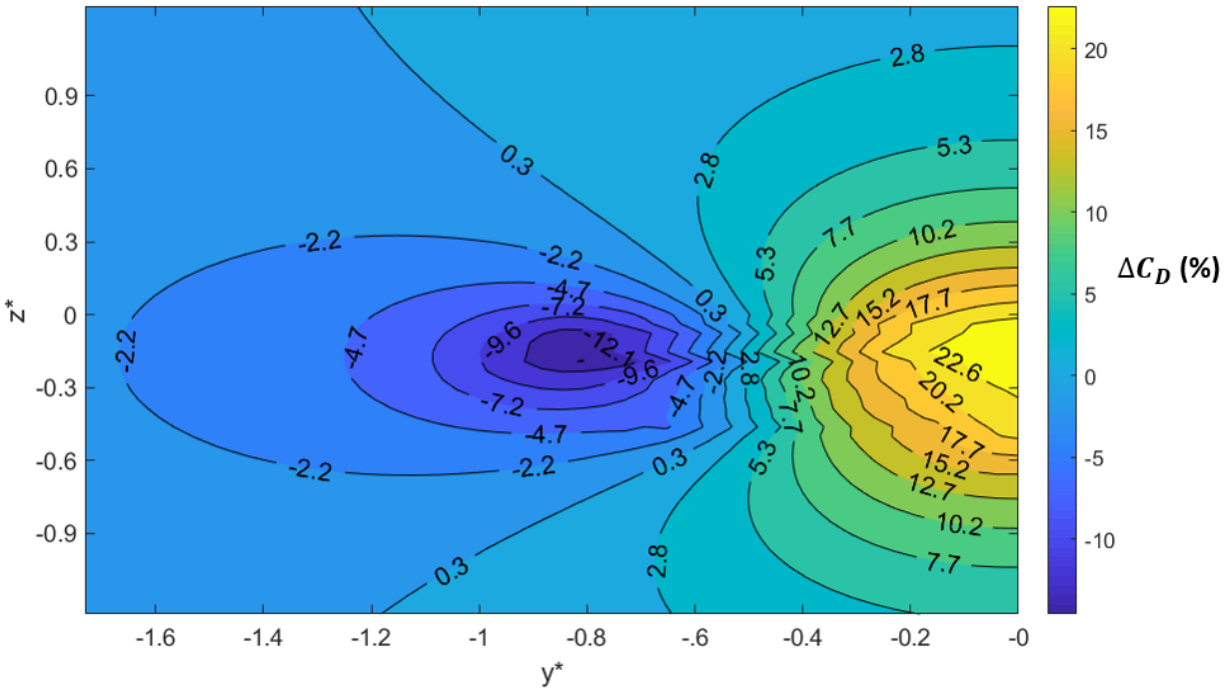

Figure 11 – Drag benefit map for a follower aircraft in terms of z^* and y^*, and in relation to the position of the wake-generating aircraft $(y^*, z^* = 0)$

The sweet spot, or the area where the performance benefits can be maximised has been predicted at $y^* = 0.8$ and $z^* = -0.25$. The drag reduction that can be obtained if the follower aircraft is placed there is around 12%. The neutral line, or the area with no gain or losses, starts near $y^* = 0.5$, meaning that if the follower is located further outboard it will get benefits from the formation, whereas if y^* is smaller than 0.5, there will be a drag penalty. The most detrimental area in terms of drag performance has been located at a $y^* = 0$. It is important to note that the maximum penalty (that of around 23%) is almost twice that of the highest gain, caused due to the influence of both port and starboard vortices. It is exactly due to the proximity of such beneficial and detrimental areas that contour maps, such as Figure 11 are necessary. Furthermore, these diagrams must be generated using wake models of the appropriate fidelity and interpreted with the intended use in mind. Small errors in spatial locations can produce large performance changes; here the sweet spot is only $y^* = 0.3$ away from the prejudicial area! Although the VWM approach is meant to be used as a tools for initial assessment, it has obtained a similar drag-benefit map distribution to those of Zhang et al[5]. Finally, there are some areas in Figure 11 that have no physical meaning but instead are symptoms of numerical errors. For example the sudden peaks at $z^* = 0$ level highlight the difficulties modelling the vortex core within the UVLM algorithm in the wake development phase.

Figure 12 presents the variation of induced drag for the follower aircraft as a function of y^* and z^*. Results from four cases are presented: (1) VWM with no trim corrections, (2) VWM with trimmed control deflections, (3) numerical simulations done by Slotnick et al[3] using the code DACVINE and, (4) Halaas et al[4] that uses RANS. The latter two cases were carried out as part of the $AVE program. It can be observed that VWM places the neutral line at around $y^* = 0.55$, while RANS and DACVINE define it at $y^* = 0.6$. This can be attributed to lack of modelling of complex aerodynamic interactions. This displacement of the neutral line displacement was also found by Fleischmann et al[25]. In terms

of the sweet spot location, VWM locates it at y*=0.8, in accordance with DACVINE and RANS. The last one is considered to be the most accurate simulation because it is based on high-fidelity RANS CFD.
The maximum gain predicted by VWM at the sweet spot was found to be of 15% induced drag reduction compared to the 20% estimated by DACVINE and the 12% predicted via RANS simulations. This highlights the difficulties that arise when modelling extended formation flight. These two approaches[3] [4] utilise the same aircraft geometry but differ from each other by more than 8%. VWM on the other hand falls in the middle. Due to the omission of the parasite drag component, the difference between VWM trimmed and no trimmed is almost negligible.

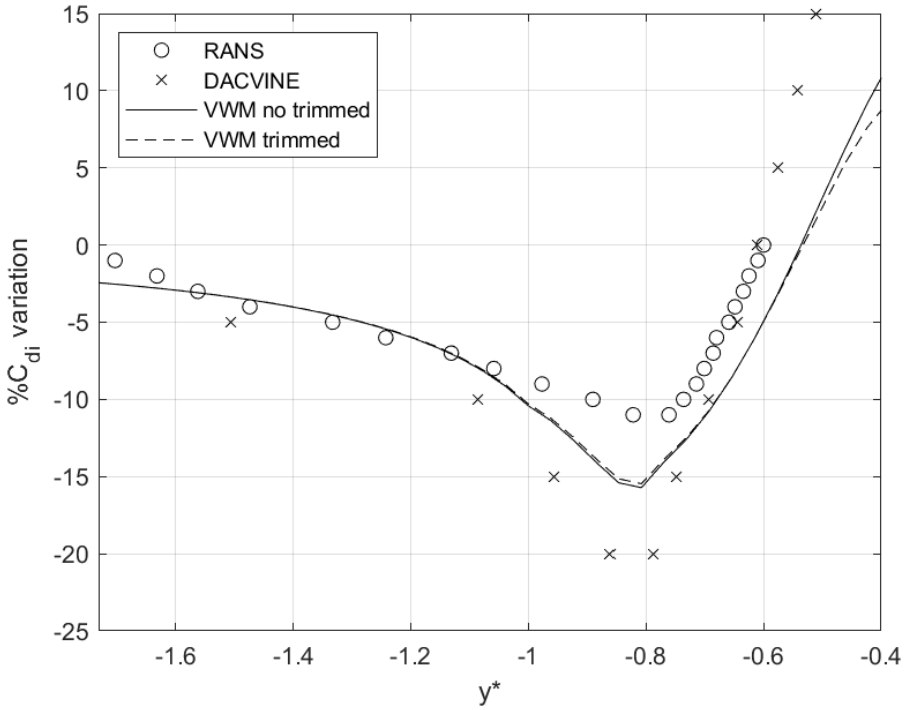

Figure 12 – Comparison of induced drag variations.

A large number of reasons can explain these differences, and in the interest of brevity only the major factors are discussed here. First of all, the reader should note that RANS is computing a drag component in addition to $C_{D,i}$, defined by the authors as residual value, that we are not considering. It is expected that this drag component will reduce the performance improvements, and hence the lower maximum gains obtained by RANS in Figure 12. . Secondly, the simplistic assumptions followed in this study, flat-plate geometry, UVLM modelling of the wake etc. are the main sources of variations between VWM results and those found in the literature.
Although the absolute values of most of the parameters differ from other high-fidelity or experimental studies, VWM has been able to provide a degree of accuracy (in terms of trends) not expected from such a simple approach and at a much lower computational expense.

5. Conclusions

This paper has outlined a computationally cheap low fidelity approach for assessing extended formation flight which relies on UVLM based reduced order aerodynamics for wake generation, coupled with methods for wake decent and decay. A simple approach called the Virtual Wing Method or VWM is then applied to estimate the effects of this wake on a follower aircraft and then estimate potential gains that can be extracted from the wake field generated by a lead aircraft. The wake descent model implemented in this study has been compared to numerous numerical and experimental data available in the public domain and shown to perform a sufficiently accurate modelling of the wake trajectory; at least for mild atmospheric conditions. The test case for this study was chosen such that

the results could be directly related to the USAF $AVE program and therefore, the simulations considered an extended formation of two C-17 aircraft. Although a number of simplifications were made when modelling aircraft geometry, VWM has been able to capture the main trends of the effects imposed on the follower aircraft by the wake during the encounter phase. Indeed the absolute values do differ from results from other high-fidelity studies, but it is shown that VWM can accurately predict the location of important features: such as the neutral points or the regions of peak benefit. Results from VWM are then used to develop a drag benefit map at a relatively low computational cost. It is also shown that this approach estimates the location of the sweet spot within 10% of those predicted by higher-fidelity approaches with a potential drag reduction of up to 12%. The results also demonstrate that the benefits can be greatly reduced if the follower aircraft is positioned in other regions of the benefit map: in the worst case a drag penalty of up to 22% is predicted. In conclusion, this study has shown the potential use of a computationally inexpensive approach to perform rapid assessments of extended formation flight operations to quickly provide initial estimates of potential benefits and highlight potential risks.

6. Contact Author Email Address

r.vilumbrales-garcia@soton.ac.uk

7. Copyright Statement

References

[1] P. B. S. Lissaman and C. A. Schollenberger. Formation flight of birds. *Science*, 168(3934):1003–1005, 1970.

[2] H. Weimerskirch, J. Martin, Y. Clerquin, P. Alexandre, and S. Jiraskova. Energy saving in flight formation. *Nature*, 413(6857):697–698, 2001.

[3] J. Slotnick, R. Clark, D. Friedman, Y. Yadlin, and D. Yeh. Computational aerodynamic analysis for the formation flight for aerodynamic benefit program. In *52nd AIAA Aerospace Sciences Meeting*, January 2014.

[4] D. J. Halaas, S. R. Bieniawski, B. T. Whitehead, T. Flanzer, and W. B. Blake. Formation flight for aerodynamic benefit simulation development and validation. In *52nd AIAA Aerospace Sciences Meeting*, January 2014.

[5] Q. Zhang and H. H. T. Liu. Aerodynamics modeling and analysis of close formation flight. *Journal of Aircraft*, 54(6):2192–2204, 2017.

[6] T. Flanzer, S. Bieniawski, and W. Blake. Operational analysis for the formation flight for aerodynamic benefit program. In *Proceedings of the AIAA 52nd Aerospace Sciences Meeting*, number AIAA2014-1460, 2014.

[7] S. Bieniawski and R. Clark. Summary of flight testing and results for the formation flight for aerodynamic benefit program. In *52nd AIAA Aerospace Sciences Meeting*, January 2014.

[8] G. C. Greene. Approximate model of vortex decay in the atmosphere. *Journal of Aircraft*, 23(7):566–573, 1986.

[9] T. Sarpkaya. New model for vortex decay in the atmosphere. *Journal of Aircraft*, 37(1):53–61, 2000.

[10] F. Holzäpfel. Probabilistic two-phase wake vortex decay and transport model,. *Journal of Aircraft*, 40(2):323–331, 2003.

[11] Fred H. Proctor. Numerical simulation of wake vortices measured during theidaho falls and memphis field programs. In *14th AIAA Applied Aerodynamic Conference*, number 96-2496, 1996.

[12] S. A. Ning. *Aircraft Drag Reduction Through Extended Formation Flight*. PhD thesis, Stanford University, August 2011.

[13] B. E. Smith and J. C. Ross. Application of a panel method to wake-vortex interaction and comparison with experimental data. Technical Report NASA-TM-88337, National Aeronautics and Space Administration, September 1987.

[14] G.R. Hough. Remarks on vortex-lattice methods. *Journal of Aircraft*, 10(5):314–317, 1973.

[15] V.J. Rossow. Validation of vortex-lattice method for loads on wings inlift-generated wakes. *Journal of Aircraft*, 32(6):1254–1262, 1995.

[16] Elsa M. Cardenas, Pedro J. Boschetti, and Andrea Amerio. Stability and flying qualities ofan unmanned airplane usingthe vortex-lattice method. *Journal of Aircraft*, 46(4):1461–1464, 2009.

[17] Fabiano Hernandes and Paulo A. O. Soviero. Unsteady aerodynamic coefficients obtained by a compressible vortex lattice method. *Journal of Aircraft*, 46(4):1291–1301, 2009.

[18] J. Katz and A. Plotkin. *Low-Speed Aerodynamics*. Cambridge University Press, second edition, 2001.

[19] S. C. Crow and E. R. Bate. Lifespan of trailing vortices in a turbulent atmosphere. *Journal of Aircraft*, 13(7):476–482, 1976.

[20] M. Drela. *Flight Vehicle Aerodynamics*. The MIT Press, 2014.

[21] S. D. Campbell, T. J. Dasey, R. E. Freehart, R. M. Heinrichs, M. P. Matthews, G. H. Perras, and G. S. Rowe. Wake vortex field measurement program at memphis, tennessee - data guide. Technical Report NASA-CR-201690, National Aeronautics and Space Administration, April 1997.

[22] M. V. Cook. *Flight Dynamics Principles*. Butterworth-Heinemann, third edition, 2012.

[23] S. F. Hoerner. *Fluid-Dynamic Drag*. Hoerner Fluid Dynamics, 1965.

[24] T. Misaka, F. Holzäpfel, and T. Gerz. Large-eddy simulation of aircraft wake evolution from roll-up until vortex decay. *AIAA Journal*, 53(9):2646–2670, 2015.

[25] D. Fleischmann and M. Lone. Analysis of wake surfing benefits using a fast unsteady vortex lattice method. In *AIAA SciTech Forum 2019*, 2019.